University of Groningen

Detection of extragalactic H3O+

van der Tak, Floris; Aalto, Susanne; Meijerink, Rowin

IMPORTANT NOTE: You are advised to consult the publisher's version (publisher's PDF) if you wish to cite from it. Please check the document version below.

Document Version
Publisher's PDF, also known as Version of record

[Link to publication in University of Groningen/UMCG research database](#)

LETTER TO THE EDITOR

Detection of extragalactic H_3O^+

F.F.S. van der Tak[1,2], S. Aalto[3], and R. Meijerink[4]

[1] SRON Netherlands Institute for Space Research, Landleven 12, 9747 AD Groningen, The Netherlands; e-mail: `vdtak@sron.nl`
[2] Kapteyn Astronomical Institute, University of Groningen, The Netherlands
[3] Onsala Space Observatory, Chalmers University of Technology, 43992 Onsala, Sweden
[4] Astronomy Department, University of California, 601 Campbell Hall, Berkeley, CA 94720, USA

ABSTRACT

Context. The H_3O^+ molecule probes the oxygen chemistry and the ionization rate of dense circumnuclear gas in galaxies.
Aims. Recent H_3O^+ observations show variations in the cosmic-ray ionization rate by factors of >10 within our Galaxy.
Methods. Using the JCMT, we have observed the 364 GHz line of p-H_3O^+ in the centers of M82 and Arp 220.
Results. In Arp 220, the line profile suggests that the emission originates in the Western nucleus. In M 82, both the eastern molecular peak and the circumnuclear region contribute to the emission. The derived column densities, abundances, and H_3O^+ / H_2O ratios indicate ionization rates similar to or even exceeding that in the Galactic Center.
Conclusions. Model calculations of the chemistry of irradiated molecular gas indicate a likely origin of this high ionization rate in the extended, evolved starburst of M82. In contrast, irradiation by X-rays from the AGN disk is the most likely model for Arp 220.

Key words. galaxies: starburst; galaxies: active; radio lines: galaxies; ISM: molecules

1. Introduction

Starbursts and active galaxies often host large masses of molecular gas and dust in their inner kpc. Gravitational interaction or merging cause the funneling (via bars) of the gas towards the center. The average gas surface- and number densities are significantly higher (by several orders of magnitude) than in the more extended disks. The nuclear molecular gas is often found in tori, feeding the activity and thus controlling its evolution. The triggering and turn-off mechanisms of the activity are dependent on the properties of the gas, which are still poorly known, in particular the fraction of the gas at high temperature and density. Observations of the molecular gas properties are starting to show great promise not only in allowing us to model the evolution of the starburst, but also in helping to identify and analyze the type of activity lurking in very deeply obscured galactic nuclei. Here, dust extinction is high enough to quench emission even down to the mid-infrared. For reviews of this subject, see Sanders & Mirabel (1996) and Gao & Solomon (2004).

The star formation rates in the nuclei of nearby galaxies are measured best at (sub-)millimeter wavelengths, where extinction is negligible and where a rich spectrum of dust continuum and molecular lines allows us to measure fundamental parameters of star-forming matter such as mass, temperature, and density (e.g., Aalto et al. 2002). However, existing observations are mostly at millimeter wavelengths and thus limited to relatively low temperatures and densities. The excellent transmission of sites like Mauna Kea and Chajnantor enables observation of the H_3O^+ molecule, which has a twofold importance.

First, the H_2O molecule acts as a natural filter for selecting hot ($\gtrsim 100\,K$) gas, and therefore traces different regions than CO and other molecules commonly studied from low-altitude sites. The chemistry of this filtering is the evaporation of icy grain mantles at $T \approx 100\,K$ (Van der Tak et al. 2006a). Other molecules evaporating from grain mantles are not as abundant as H_2O. The H_3O^+ molecule is an excellent proxy for H_2O, which cannot be observed in thermal lines from the ground at redshifts below 0.01. In contrast to HDO whose ratio to H_2O strongly depends on ambient conditions, the chemical relation between H_3O^+ and H_2O is well-understood and the relevant reactions have been measured in the laboratory (Phillips et al. 1992). Thus, observations of H_3O^+ are useful probes of the gas distribution and kinematics in the warm and dense nuclei of active galaxies.

Second, the high proton affinity of H_2O makes H_3O^+ a key ion in the oxygen chemistry of dense molecular gas. Combined with information on the H_2O abundance, observations of H_3O^+ may be used to trace the ionization rate of dense circumnuclear clouds by cosmic rays (produced in supernovae, i.e., starbursts) and X-rays (from an AGN). The ionization rate of this gas is a fundamental parameter for its dynamics, because it regulates the efficiency of magnetic support against gravitational collapse. Recent APEX observations of H_3O^+ show that the cosmic-ray ionization rate in the Sgr B2 cloud near the Galactic center is ~10× higher than in star-forming regions at 1–4 kpc from the Sun (Van der Tak et al. 2006b).

Motivated by the results of H_3O^+ observations in our Galaxy, we searched for H_3O^+ emission in two prototypical active galaxies: M82 and Arp 220. At a distance of 4 Mpc, M82 is the prototype evolved starburst, with a large H_2 mass, where many molecules were seen for the first time outside our Galaxy, including CO^+, a tracer of strong irradiation of molecular gas (Fuente et al. 2006). The molecular emission can be roughly divided into two prominent lobes of molecular emission, separated

by 30″, which is interpreted as a 400 pc rotating molecular ring. There is also molecular gas in the nucleus, which is best seen in high-J CO lines or in high-density tracer emission, such as HCO (e.g., García-Burillo et al. 2002).

The prototypical ultraluminous galaxy Arp 220 (d = 72 Mpc), where water lines have been detected (González-Alfonso et al. 2004; Cernicharo et al. 2006), is a merger of two gas-rich disk galaxies. Significant ($\gtrsim 10^9 \, M_\odot$) molecular gas has gathered in two nuclei (east and west) that have not yet merged into one. The two nuclei are separated by 1″ and are surrounded by a 5″ extended disk of molecular gas. The bulk of the molecular emission from Arp 220 is emerging from this region (e.g., Sakamoto et al. 1999), and the JCMT beam covers all of it. Arp 220 has a rich chemistry with surprisingly bright HNC 3–2 line emission, outshining HCN 3–2 by a factor of 2, which indicates unusual chemical or excitational circumstances. High-resolution observations reveal that the HNC emission is emerging from warm gas ($T_k > 40$ K) near the western nucleus (Aalto 2007).

2. Observations

The 3_2^+–2_2^- line of H₃O⁺ was observed during April 26-28, 2007, with the James Clerk Maxwell Telescope (JCMT)[1] under program M07AN03. In the 345 GHz window, the telescope has a beam size of 14″ and a main beam efficiency of 70%, as determined by the telescope staff and verified by scans of Mars at the end of each night. One of the central pixels of the Heterodyne Array Receiver Program (HARP) was used as front end, with receiver temperatures of ∼120 K at our observing frequency of ∼360 GHz. The back end was the Auto-Correlation Spectrometer and Imaging System (ACSIS), providing 1.0 GHz bandwidth in 2048 channels. The weather was excellent throughout, with water vapour columns of $\lesssim 1$ mm, corresponding to a zenith opacity of $\tau \lesssim 0.05$ at 225 GHz. System temperatures were 300-400 K for M82 and 200-300 K for Arp 220, which reaches higher elevations and whose larger redshift puts the line at a frequency with better atmospheric transmission. Double beam switching at a rate of 1 Hz was used with an offset of 120″ in azimuth, which led to flat, stable baselines. Integration times (on+off) are 8.2 hrs for Arp 220 and 6.5 hrs for M82, resulting in rms noise levels of $T_A^* = 2$-3 mK per 8 km s⁻¹ channel. Telescope pointing was checked every hour on the CO line emission of nearby AGB stars and always found to be within 2″. The telescope z-focus was checked on bright AGB stars at the beginning of the night (after sunset) and around midnight, and corrected by 0.1-0.2 mm. The bright AGB stars were also used to take standard spectra, and the results lead us to believe that the calibration of the data is accurate to ∼10%.

Initial reduction of the data was done with the Starlink package, and the final analysis performed in Class. We inspected the individual scans, summing the good ones, and subtracted linear baselines. The identification of the spectral feature as H₃O⁺ is secure, since the standard molecular line catalogs (Pickett et al. 1998; Müller et al. 2001) do not list any other plausible candi-

Table 1. Measured line parameters with 1σ errors in brackets in units of the last decimal.

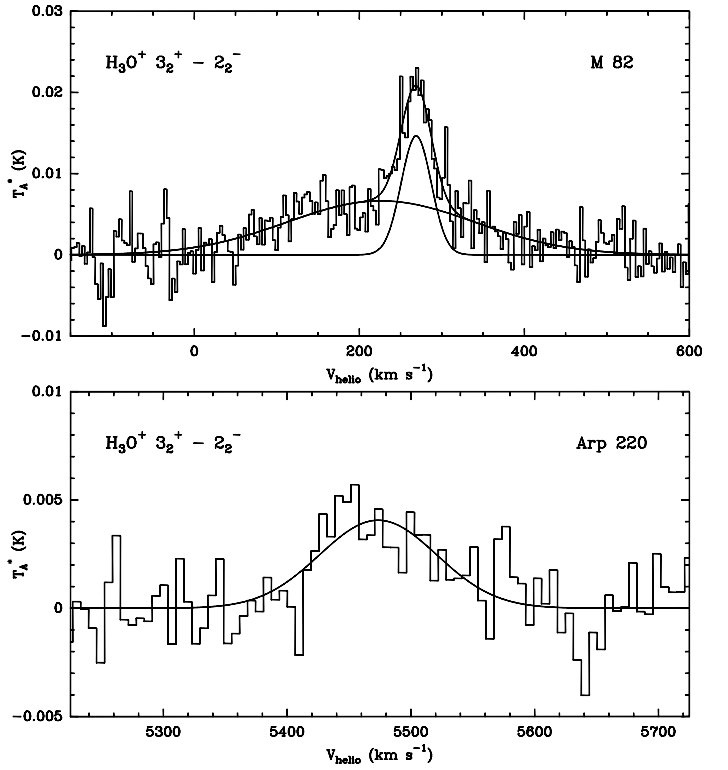| Source	α(J2000) hh mm ss	δ(J2000) ° ′ ″	T_A^* mK	V_{hel} km s⁻¹	ΔV km s⁻¹
M82	09:55:52.19	+69:40:48.8	15(2)	269(2)	43(5)
	broad component:		6.5(6)	224(11)	261(23)
Arp 220	15:34:57.23	+23:30:11.5	4.1(6)	5473(8)	113(20)

Fig. 1. Spectra of the H₃O⁺ 3_2^+–2_2^- line toward M82 (top) and Arp 220 (bottom), observed with the JCMT.

dates at this frequency, and the attenuation of the image sideband is better than 10 dB. After smoothing the data to a velocity resolution of 8-16 km s⁻¹, line parameters were extracted by fitting Gaussian profiles to the spectra. The final spectra are shown in Fig. 1 and the line parameters listed in Table 1. Throughout this paper, velocities are in the heliocentric frame and redshift is computed using the radio convention.

3. Results

Emission due to H₃O⁺ is clearly detected towards the nuclei of both M82 and Arp 220. The signal-to-noise ratio on the line profiles is high enough to address the location of the emission within the galaxies. In the case of Arp 220, the line profile is single-peaked and similar to that of CH₃OH (Martín-Pintado 2007). The emission peak at $V_{hel} \approx 5500$ km s⁻¹ indicates an origin in the western nucleus, which is also where the HNC 3–2 emission peaks in recent interferometric images (Aalto et al. 2007). In the case of M82, the emission peak at $V_{hel} \approx 300$ km s⁻¹ suggests an origin in the eastern molecular peak at about 12″ (240 pc) from the nucleus, which is where the CO emission

peaks (Tilanus et al. 1991) and where CO^+ and CH_3OH are also located (Fuente et al. 2006; Martín et al. 2006). The profile almost extends to $V_{hel} \approx 200\,km\,s^{-1}$, which suggests that significant H_3O^+ is also present in the central region of the galaxy, as found before for N_2H^+ (Mauersberger & Henkel 1991). In fact, a single Gaussian profile does not give a good fit to the M82 spectrum. Figure 1 shows a decomposition of the profile into two Gaussians, where the narrow component represents H_3O^+ in the eastern molecular peak of M82 and the broad component either the more widely-distributed molecular gas or the contribution from the nucleus. This decomposition of the line profile may not be unique, but serves to illustrate the existence of multiple H_3O^+ components in the nucleus of M82. Although the JCMT beam is too small to cover the eastern lobe of M82 while pointing at the center, it is possible that we are picking up emission from the inner side of the lobe. The other HARP pixels do not cover the lobe either, but future fully-sampled maps will reveal the spatial distribution of H_3O^+ in M82.

To estimate the column density of H_3O^+ towards our sources from the integrated line intensities (Table 1), we adopt a main beam efficiency of 70% and regard the expected kinetic temperature of ~ 100 K as an upper limit to the excitation temperature (T_{ex}). For $T_{ex} = 50 - 100$ K, the column density of p-H_3O^+ is $0.7 - 1.3 \times 10^{13}\,cm^{-2}$ for Arp 220 and $3.0 - 5.5 \times 10^{13}\,cm^{-2}$ for M82. The total beam-averaged column density of H_3O^+ is $2 - 3$ times higher, because the ortho to para ratio of H_3O^+ drops from the high-temperature limit of $o/p = 1$ at $T \gtrsim 100$ K to $o/p \gtrsim 2$ at $T \lesssim 50$ K. The following discussion adopts the intermediate case of $o/p = 1.5$; we refer to Phillips et al. (1992) and Van der Tak et al. (2006b) for further discussion of H_3O^+ radiative transfer.

Unlike for lower-frequency lines of heavier molecules that are excited by collisions, the excitation temperature of H_3O^+ probably reflects the colour temperature (T_C) of the far-infrared radiation field rather than the kinetic temperature of the molecular gas. The low reduced mass of the H_3O^+ molecule makes its excitation very sensitive to radiative pumping by dust (Phillips et al. 1992; Van der Tak et al. 2006b). Calculations with the RADEX non-LTE radiative transfer program (Van der Tak et al. 2007) using molecular data from the LAMDA database (Schöier et al. 2005) indicate that the coupling between T_{ex} and T_C holds as long as $T_C > 30$ K and that the measured line is optically thin under these conditions. We assume a filling factor of the dust radiation field of unity, representing the case that the gas and dust are well-mixed.

The beam-averaged H_3O^+ column density in Arp 220 is almost certainly an underestimate of its source-averaged value, because the emission is unlikely to be as extended as $14''$. First, the molecular gas traced by the CO 2–1 emission is concentrated in two nuclei of diameter 300 pc each (Sakamoto et al. 1999). Recent high-resolution work on HNC 3–2 (Aalto et al. 2007) further shows that the dense gas is concentrated towards the western nucleus with a source size of 0.7 arcsec (260 pc). Second, since H_3O^+ is excited by infrared radiation, its emission may follow the infrared light distribution. From 3–25 μm Keck observations, Soifer et al. (1999) find a size of $0.73''$ at 25 μm. They derive a size of $2''$ at 100 μm, which seems a firm upper limit to the H_3O^+ source size. Furthermore, the absence of a double-peaked profile from the two nuclei in our data suggests that the emission is located on one of the two nuclei and does not

Table 2. Source-averaged column densities [cm^{-2}] of H_2, H_2O, and H_3O^+.

Source	$N(H_2)$	$N(H_2O)$	$N(H_3O^+)$	Refs.
M82	1×10^{23}	$< 2 \times 10^{14}$	1.1×10^{14}	[1,2,3]
Arp 220	1×10^{24}	2×10^{17}	1.0×10^{16}	[4,5,6]

References: [1] Mao et al. (2000); [2] Wilson et al. (2007);
[3] This work; [4] Downes & Eckart (2007);
[5] González-Alfonso et al. (2004); [6] This work.

cover the full extent of the CO emission. We thus adopt a source size of $0.7''$, which must of course be verified at high resolution.

In the case of M82, the dense molecular gas is distributed over many clumps as shown by high-resolution CO and HCO images (García-Burillo et al. 2002). These clumps are grouped in three lobes (east, middle, and west) separated by $\approx 15''$ (300 pc), with significant emission coming from the medium in between. Our JCMT beam is pointed to a position close to the central lobe, so that a significant fraction of the beam is probably filled with H_3O^+ emission.

Table 2 reports the column densities of H_3O^+, H_2O, and H_2 in our sources, as taken from this work and the literature. The values refer to a $\approx 15''$ area for M82 and a $\approx 0.7''$ area for Arp 220. Our adopted $N(H_2)$ toward Arp 220 is $10\times$ below the peak value reported by Downes & Eckart (2007) for a $0.2''$ area, so that it is representative of our assumed H_3O^+ source size of $0.7''$. The table shows that the abundance of H_3O^+ relative to H_2 is ~ 2–10×10^{-9} in these sources. These values are much higher than the typical value for Galactic star-forming cores (Phillips et al. 1992) and at or above the value of 3×10^{-9} in the Sgr B2 cloud at the Galactic center (Van der Tak et al. 2006b). The ionization rate of the molecular gas in the nuclei of Arp 220 and M82 thus seems comparable to the value in the Galactic center. This conclusion is supported by the H_3O^+/H_2O ratio of 1/50 that we find for Arp 220, which is similar to the value of 1/20 for the Galactic center. No useful estimate of this ratio can be made for M82: the Odin data quoted in Table 2 have a beam size of $2'$ and thus sample a very different gas volume than our JCMT data. Note that our estimated H_3O^+ abundance in Arp 220 is somewhat hampered by source size uncertainties.

4. Discussion

The column densities of H_3O^+, H_2O, and H_2 in Table 2 and their ratios are compared to chemical models of clouds irradiated by either far-UV or X-ray photons. Far-UV dominated clouds are called photon-dominated regions (PDRs) and the other type X-ray dominated regions (XDRs). The thermal and chemical structures of PDRs and XDRs are quite different, because the absorption cross section for X-rays is much lower than for far-UV. The ionization fraction in XDRs can be as high as $x_e = 10^{-2} - 10^{-1}$, while in PDRs, it is 10^{-4} at most. Furthermore, in XDRs, larger parts of the cloud can be kept at a high temperature. For an elaborate discussion of the differences between PDRs and XDRs we refer to Meijerink & Spaans (2005) where the codes are described. The grid of models by (Meijerink et al. 2007) is used to look for the best match to our observations. For the PDR models, we also consider an elevated cosmic-ray ion-

ization rate of $\zeta = 5.0 \times 10^{-15}$ s^{-1}. As reference, we take the radiation field found by Spaans & Meijerink (2007) for M82 to model the CO$^+$ abundance found by Fuente et al. (2006). Their best-fitting model was an XDR with a density of $n = 10^5$ cm^{-3} and an incident X-ray flux of $F_X = 5.1$ erg s^{-1} cm^{-2} ($G_0=10^{3.5}$). Using this density and radiation field, the model predicts the column densities listed in Table 3. The chemical structure of the model is shown in Fig. 2. Models for volume densities far below $n = 10^5$ cm^{-3} fail to produce appreciable H$_3$O$^+$ abundances, which makes it unlikely that the origin of the observed emission is in interclump gas, seen e.g. as the $N_H=10^{20}$ cm^{-2} CO component in M82 (Mao et al. 2000).

Table 3 shows that the H$_3$O$^+$ column density observed in M82 may be produced in either XDR or in the high-ζ PDR. The H$_3$O$^+$/H$_2$ ratio in M82 is overproduced in the XDR models and underproduced in the standard PDR, but agrees very well with the high-ζ model. None of the models reproduce the observed H$_3$O$^+$/H$_2$O ratio in M82, probably because the observations refer to very different volumes. We conclude that the M82 data are matched best by the PDR model with enhanced cosmic-ray flux. In contrast, the X-ray models do best in reproducing the observations of Arp 220. The H$_3$O$^+$ column density of 10^{16} cm^{-2} is matched by an XDR model with $N_H=10^{23}$ cm^{-2}, scaled up by a factor 10, for either value of F_X. The H$_3$O$^+$ abundance of 1×10^{-8} is matched by the high-F_X model for low N_H or the low–F_X model for high N_H. The H$_3$O$^+$/H$_2$O ratio is matched by an XDR of either F_X, where low values of N_H are preferred. Nevertheless, a contribution by the eastern nucleus is implausible because of its low mass of dense gas and its low infrared brightness.

In the context of galactic nuclei, a PDR model represents a starburst, where the far-UV is produced by young massive stars and the cosmic rays in supernova remnants. The pure PDR thus stands for a young starburst and the high-ζ model for an evolved one. The XDR models represent the much harder radiation environment of an AGN, such as the accretion disk of a supermassive black hole. We find that the observations of M82 are matched by a high-ζ PDR, i.e., an evolved starburst. This conclusion is consistent with earlier models of this source (Förster Schreiber et al. 2003). Our H$_3$O$^+$ observations do not require X-ray irradiation as in the case of CO$^+$ (Spaans & Meijerink 2007).

The fact that the XDR models give conflicting requirements on the N_H value toward Arp 220 may well be due to the unusual geometry of this object. The emerging picture of the western nucleus of Arp 220 is that there is a 35 pc optically thick dust disk surrounding what could potentially be an active nucleus. The dust disk is warm ($T_D \approx 170$ K) and has a peak H$_2$ column density of $\approx10^{25}$ cm^{-2}. Hence X-rays, optical, and even infrared emission from the nucleus itself will be absorbed (Downes & Eckart 2007). Surrounding this warm dust disk is a cooler ($T_k \approx 50$ K) molecular disk or torus causing CO 2–1 absorption features towards the hotter nuclear dust disk in the line of sight. Most of the observed starburst activity appears to be associated with the rotating disk/torus surrounding the nuclear dust disk. Future modeling efforts of H$_3$O$^+$ in Arp 220 should take this special geometry into account. However, high-resolution observations are needed to constrain these models. It is possible for example that the disk causes both H$_3$O$^+$ emission and absorption along the line of sight.

In the near future, the HIFI heterodyne spectrometer onboard ESA's *Herschel* space observatory will be able to measure H$_2$O

Table 3. Results of PDR / XDR models.

N_H cm^{-2}	N(H$_2$) cm^{-2}	N(H$_3$O$^+$) cm^{-2}	N(H$_2$O) cm^{-2}	H$_3$O$^+$/H$_2$	H$_3$O$^+$/H$_2$O
XDR $F_X = 5.1$ erg s^{-1} cm^{-2}					
1×10^{22}	1.4×10^{21}	6.1×10^{13}	5.6×10^{15}	4.3×10^{-8}	1.1×10^{-2}
3×10^{22}	7.9×10^{21}	1.9×10^{14}	2.2×10^{16}	2.5×10^{-8}	8.7×10^{-3}
1×10^{23}	3.9×10^{22}	3.6×10^{14}	5.8×10^{16}	9.2×10^{-9}	6.1×10^{-3}
XDR $F_X = 16$ erg s^{-1} cm^{-2}					
1×10^{22}	1.7×10^{20}	3.1×10^{12}	1.7×10^{14}	1.8×10^{-8}	1.8×10^{-2}
3×10^{22}	2.3×10^{21}	1.5×10^{14}	1.2×10^{16}	6.6×10^{-8}	1.2×10^{-2}
1×10^{23}	2.5×10^{22}	8.4×10^{14}	8.9×10^{16}	3.4×10^{-8}	9.4×10^{-3}
PDR $G_0=10^{3.5}$ $\zeta = 5.0 \times 10^{-17}$ s^{-1}					
1×10^{22}	4.6×10^{21}	2.3×10^{11}	1.6×10^{14}	5.0×10^{-11}	1.4×10^{-3}
3×10^{22}	1.5×10^{22}	1.7×10^{12}	1.6×10^{15}	1.2×10^{-10}	1.1×10^{-3}
1×10^{23}	5.0×10^{22}	6.8×10^{12}	6.6×10^{15}	1.4×10^{-10}	1.0×10^{-3}
PDR $G_0=10^{3.5}$ $\zeta = 5.0 \times 10^{-15}$ s^{-1}					
1×10^{22}	4.6×10^{21}	9.2×10^{12}	2.7×10^{15}	2.0×10^{-9}	3.4×10^{-3}
3×10^{22}	1.4×10^{22}	4.3×10^{13}	1.3×10^{16}	2.9×10^{-9}	3.2×10^{-3}
1×10^{23}	4.9×10^{22}	1.6×10^{14}	5.1×10^{16}	3.2×10^{-9}	3.1×10^{-3}

and H$_3$O$^+$ lines around 1 THz and make accurate estimates of the H$_2$O/H$_3$O$^+$ ratios in many sources. These data will allow a much better understanding of the ionization rates of molecular regions inside and outside our Galaxy. Future additions to the model include the effects of freeze-out onto and desorption from dust grains, the effect of metallicity changes, and (especially for the Arp 220 merger) the time dependence introduced by shocks.

References

Aalto, S. 2007, in Science with ALMA, ed. J. Cernicharo, in press
Aalto, S., Polatidis, A., Hüttemeister, S., & Curran, S. 2002, A&A, 381, 783
Aalto, S., Spaans, M., Wiedner, M. C., & Hüttemeister, S. 2007, A&A, 464, 193
Cernicharo, J., Pardo, J. R., & Weiss, A. 2006, ApJ, 646, L49
Downes, D. & Eckart, A. 2007, A&A, 468, L57
Förster Schreiber, N., Genzel, R., Lutz, D., & Sternberg, A. 2003, ApJ, 599, 193
Fuente, A., García-Burillo, S., Gerin, M., et al. 2006, ApJ, 641, L105
Gao, Y. & Solomon, P. M. 2004, ApJ, 606, 271
García-Burillo, S., Martín-Pintado, J., Fuente, A., et al. 2002, ApJ, 575, L55
González-Alfonso, E., Smith, H., Fischer, J., et al. 2004, ApJ, 613, 247
Mao, R. Q., Henkel, C., Schulz, A., et al. 2000, A&A, 358, 433
Martín, S., Martín-Pintado, J., & Mauersberger, R. 2006, A&A, 450, L13
Martín-Pintado, J. 2007, in Molecules in Space, ed. F. Combes, in press
Mauersberger, R. & Henkel, C. 1991, A&A, 245, 457
Meijerink, R. & Spaans, M. 2005, A&A, 436, 397
Meijerink, R., Spaans, M., & Israel, F. P. 2007, A&A, 461, 793
Müller, H., Thorwirth, S., Roth, D., & Winnewisser, G. 2001, A&A, 370, L49
Phillips, T. G., van Dishoeck, E. F., & Keene, J. 1992, ApJ, 399, 533
Pickett, H. M., Poynter, I. R. L., Cohen, E. A., et al. 1998, JQSRT, 60, 883
Sakamoto, K., Scoville, N. Z., Yun, M. S., et al. 1999, ApJ, 514, 68
Sanders, D. B. & Mirabel, I. F. 1996, ARA&A, 34, 749
Schöier, F., van der Tak, F., van Dishoeck, E., & Black, J. 2005, A&A, 432, 369
Soifer, B. T., Neugebauer, G., Matthews, K., et al. 1999, ApJ, 513, 207
Spaans, M. & Meijerink, R. 2007, ApJ, 664, L23
Tilanus, R. P. J., Tacconi, L. J., Sutton, E. C., et al. 1991, ApJ, 376, 500
Van der Tak, F., Walmsley, C., Herpin, F., et al. 2006a, A&A, 447, 1011
Van der Tak, F. F. S., Belloche, A., Schilke, P., et al. 2006b, A&A, 454, L99
Van der Tak, F. F. S., Black, J. H., Schöier, F. L., et al. 2007, A&A, 468, 627
Wilson, C. D., Booth, R. S., Olofsson, A. O. H., et al. 2007, A&A, 469, 121
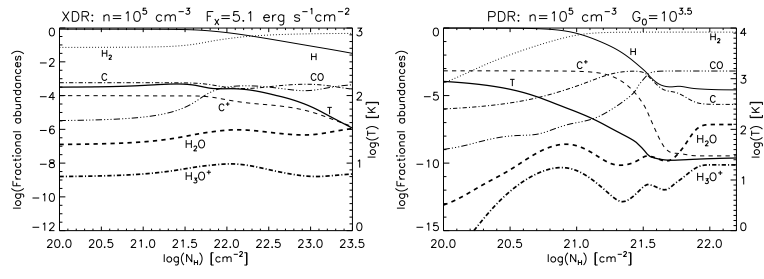
Fig. 2. Calculated chemical structure of XDR (top) and PDR (bottom) models
.